Applied Catalysis B: Environmental 174–175 (2015) 126–135

Contents lists available at ScienceDirect

Applied Catalysis B: Environmental

journal homepage: www.elsevier.com/locate/apcatb

Influence of Pt particle size and Re addition by catalytic reduction on aqueous phase reforming of glycerol for carbon-supported Pt(Re) catalysts

Aysegul Ciftci, D.A.J. Michel Ligthart, Emiel J.M. Hensen*

Schuit Institute of Catalysis, Eindhoven University of Technology, P.O. Box 513, 5600 MB Eindhoven, The Netherlands

ARTICLE INFO

Article history:
Received 5 December 2014
Received in revised form 16 February 2015
Accepted 20 February 2015
Available online 21 February 2015

Keywords:
Aqueous phase reforming
Site requirement
PtRe
Bimetallics
Catalytic reduction

ABSTRACT

We investigated the influence of Pt particle size and the addition of Re in carbon-supported catalysts in the aqueous phase reforming (APR) of glycerol. Pt nanoparticles with averaged sizes of 1.2, 1.6, 2 and 4.2 nm were obtained by reduction at increasing temperatures of Pt/C. Gas-phase water–gas shift (WGS) and acetaldehyde decomposition reactions were used to separately study important reaction steps in the APR mechanism. The APR H_2 turnover frequency, which was highest for 2 nm Pt particles, correlates with activity trends in the WGS reaction. The decarbonylation rate (acetaldehyde decomposition) is also highest for intermediate Pt particle size. Pt–Re nanoparticles were prepared by *in situ* catalytic reduction of $HReO_4$ on Pt/C followed by reduction at 300 °C. The APR activity after Re addition on Pt/C increased for Pt/C–Re having initial the smallest particles, but decreased for the other larger-sized Pt/C–Re catalysts. The bimetallic catalysts were much more active in the WGS reaction than their Pt-only parents. An increase in the reduction temperature to 600 °C resulted in a further increase of the WGS activities. The different ways Re addition affects APR and WGS activities of Pt/C catalysts relate to different surface site requirements for these reactions. The presence of isolated Pt atoms, whose fraction increases when the alloys are reduced at higher temperatures, is sufficient to bring about the synergetic effect between Pt and Re for the WGS reaction. For APR, on the other hand, the presence of surface ensembles of Pt atoms is essential for obtaining high C—O and C—C bond breaking rates.

1. Introduction

Processing of carbohydrate constituents of biomass in water is a promising method for generating clean energy and obtaining platform chemicals in a sustainable manner. Aqueous phase reforming (APR) of glycerol, an abundant feedstock formed as a by-product of biodiesel production, is an energy-efficient process for obtaining hydrogen, alkanes and alcohols. Besides, glycerol APR can be considered a suitable model reaction to the aqueous phase reforming of more complex biomass constituents such as polyols and sugars. Important reaction steps in the APR reaction mechanism are dehydration and decarbonylation reactions and the water–gas shift (WGS) reaction [1,2].

Because of its high activity, Pt is the most studied transition metal for liquid phase glycerol conversion reactions [1–8]. Although a significant number of studies have been devoted to the influence of the nature of the transition metal [3,9,10] and the support type [4,7,11–13], the effect of metal particle size on the overall activity and selectivity in APR reactions has received less attention. For instance, Wawrzetz et al. [2] showed that an increase of the Pt particle size from 1.1 to 2.6 nm for Pt/Al_2O_3 resulted in a decrease in the H_2 and CO_2 formation rates, while the hydrodeoxygenation rate increased. On contrary, Lehnert and Claus [6] reported for an analogous catalyst system that an increase of the Pt particle size from 1.6 to 3.1 nm led to an increase in the selectivity towards H_2 in glycerol APR; in this case, the overall glycerol conversion did not change. As with increasing particle size the surface is expected to contain more face atoms at the expense of corner and edge atoms, it was argued by these authors that adsorption of oxygenated hydrocarbons for subsequent C—C cleavage is preferred on terrace surfaces. Miyazawa et al. also reported that small Ru particles were less selective towards 1,2-PDO formation than large ones [14].

Alloying precious metals with other transition metals (Re, W, Mo) increases the overall activity in liquid phase reforming and hydrogenolysis of biomass-derived polyols [15–19]. We have previously reported about the significant synergistic effect between Pt

* Corresponding author at: Eindhoven University of Technology, P.O. Box 513, 5600 MB Eindhoven, The Netherlands. Tel.: +31 40 2475178; fax: +31 40 2455054.
E-mail address: e.j.m.hensen@tue.nl (E.J.M. Hensen).

http://dx.doi.org/10.1016/j.apcatb.2015.02.027
0926-3373/

and Re in aqueous phase reforming of glycerol and the importance of increased WGS activity to explain the synergy. A PtRe/C catalyst prepared by sequential impregnation (first Pt, then Re) with a Re/Pt ratio of 2 showed the highest activity [20]. The metal particles in a bimetallic PtRe/C catalyst prepared by incipient wetness impregnation were smaller than the particles in Pt/C.

The purpose of the current work is twofold. Firstly, we determined the influence of Pt particle size on glycerol APR. Secondly, we investigated the performance of Pt(core)–Re(shell) catalysts prepared by the catalytic reduction method for the same reaction. The catalytic reduction method involves Re deposition on pre-reduced Pt nanoparticles and has earlier been explored in the context of hydrocarbon reforming [21–23]. The bimetallic catalysts were then reduced at 300 °C and 600 °C to investigate the effect of mixing of the two metals in the nanoparticles. The catalysts were extensively characterized by H_2–TPR, TEM and XANES and EXAFS at the Pt and Re edges. Their catalytic activities were also evaluated in gas-phase WGS and acetaldehyde decomposition reactions, which serve as model reactions to better understand the underlying chemistry of the glycerol APR reaction. The structure sensitivity of these reactions are discussed.

2. Experimental methods

2.1. Preparation of catalysts

A set of Pt catalysts supported on activated carbon was prepared by the incipient wetness impregnation method. After drying the activated carbon support (Norit RX3-Extra, surface area = 1200 m^2/g, pore volume = 1.25 ml/g) at 110 °C overnight, an appropriate amount of $H_2PtCl_6{\cdot}6H_2O$ precursor was dissolved in deionized water. After impregnation of the Pt precursor, the sample was dried at 110 °C overnight. Pt/C catalysts with different average particle sizes were obtained by reducing portions of the parent catalyst at 400, 600, 800 and 1000 °C. The reduction was carried out under a 30% H_2/He flow (total 300 ml/min, ramp rate 2 °C/min) and a 4 h dwell time followed by passivation at room temperature (RT) under a ~1% O_2/He flow for 8 h. The bimetallic Pt/C–Re catalysts were prepared by addition of Re on the Pt/C catalysts (molar Pt/Re ratio of 0.5) by the *in situ* catalytic reduction method based on published literature [21–24]. Reduced and passivated Pt/C catalysts were dispersed in a 0.05 M HCl solution (32 cm^3/g catalyst) in a sealed glass reactor equipped with a magnetic stirrer. Air was removed by bubbling N_2 through the solution at RT for 1 h. In order to remove the N_2 and reduce the Pt, hydrogen was bubbled through the solution at 90 °C for 3 h. In a separate vessel, appropriate amount of Re precursor (NH_4ReO_4) was dissolved in 56 ml of 0.05 M HCl solution and stirred at RT by bubbling N_2 through the solution for 1 h in order to remove air. The Re precursor solution was added through an air-tight syringe to the Pt/C slurry under H_2 bubbling. The slurry was stirred at 90 °C for 1 h under H_2. Then the reactor was cooled to RT and purged with N_2 before being exposed to air. The catalyst was filtered and washed with 2 L of deionized water. After drying at 110 °C overnight, the material was divided into two portions. One portion was reduced at 300 °C, while the other portion was reduced at 600 °C (5 °C/min) under a 20% H_2/He flow for 2 h followed by passivation at RT under a ~1% O_2/He flow for 8 h. The passivated bimetallic catalysts are denoted as Pt/C(*X*)–Re(*Y*), where *X* and *Y* represent the reduction temperature after Pt impregnation and Re addition, respectively.

2.2. Catalyst characterization

The metal loading of the materials was determined by inductively coupled plasma atomic emission spectrometry (ICP-AES) analysis performed on a Goffin Meyvis Spectro Cirus^{ccd} apparatus. The samples were dissolved in a 3:1 HCl/HNO_3 solution.

Transmission electron micrographs (TEM) were acquired on a FEI Tecnai 20 transmission electron microscope at an acceleration voltage of 200 kV with a LaB_6 filament. Typically, a small amount of sample was ground and suspended in pure ethanol, sonicated and dispersed over a Cu grid with a holey carbon film.

Temperature programmed reduction (TPR) experiments were performed in a flow apparatus equipped with a reactor, a computer-controlled oven and a thermal conductivity detector. Typically, 25 mg catalyst was loaded in a tubular quartz reactor. The sample was reduced in a 8 ml/min flow of 4 vol% H_2/N_2, whilst heating from RT up to 800 °C (10 °C/min). The H_2 signal was calibrated using a CuO/SiO_2 reference catalyst.

X-ray absorption spectroscopy was carried out at the Dutch–Belgian Beamline (Dubble) at the European synchrotron radiation facility (ESRF), Grenoble, France (storage ring 6.0 GeV, ring current 200 mA). Data were collected at the Pt L_{III} and Re L_{III} edges in transmission mode. Energy selection was done by a double crystal Si(111) monochromator solid-state detector. Background removal was carried out by standard procedures. EXAFS analysis was then performed with EXCURVE931 on k^3-weighted unfiltered raw data using the curved wave theory. Phase shifts were derived from *ab initio* calculations using Hedin–Lundqvist exchange potentials and Von Barth ground states. Energy calibration was carried out with Pt foil. The amplitude reduction factor ${S_0}^2$ associated with central atom shake-up and shake-off effects was set at 0.99 by calibration of the first- and second shell Pt–Pt coordination numbers to 12 and 4, respectively, for the k^3-weighted EXAFS fits of the Pt foil. For the spectra recorded at the Re L_{III} edge, Re powder was fitted as the reference spectra and ${S_0}^2$ for the Re–Re shell was set as 0.75. Spectra were recorded in a stainless-steel controlled atmosphere cell. The cell was heated with two firerods controlled by a temperature controller. A thermocouple was placed close to the catalyst sample. Typically, a predetermined amount of finely grinded sample was pressed in a stainless steel holder and placed in the cell. Carbon foils were held between two carbon spacers. Gases (He and H_2) were delivered by thermal mass flow controllers. The catalyst sample was heated (10 °C/min), whilst recording XANES spectra. After reduction at 300 °C for 15 min, the sample was cooled and two EXAFS spectra were recorded. Subsequently, the sample was heated in a He flow and at 150 °C a CO flow was introduced and redirected through a controlled evaporator mixer (CEM) to obtain a feed mixture with a H_2O:CO ratio of 3. The sample was heated (10 °C/min) to 200, 250 and 300 °C. XANES and EXAFS spectra were recorded during WGS reaction.

2.3. Catalytic activity measurements

2.3.1. Glycerol aqueous phase reforming

APR reactions were carried out at 225 °C under 25 bar initial N_2 pressure using 60 g of 10 wt% aqueous glycerol solution in a 120 ml autoclave. An amount of 75 mg of reduced catalyst was loaded in the autoclave together with an appropriate amount of deaerated water in a N_2-flushed glovebag. The autoclave was purged five times with 10 bar of N_2 in order to remove air from the autoclave. A 50/50 w/w mixture of glycerol and water was charged into the reactor from an external holding vessel after the autoclave containing water and the catalyst reached the desired reaction temperature. The stirring speed was 600 rpm. Liquid samples were withdrawn by a ROLSI injector and analyzed by a Trace GC equipped using a Stabilwax column and a FID detector. Gas samples were collected online and analyzed by a Focus GC equipped with a TCD detector and CP-Porabond Q and RT-MolSieve-5A

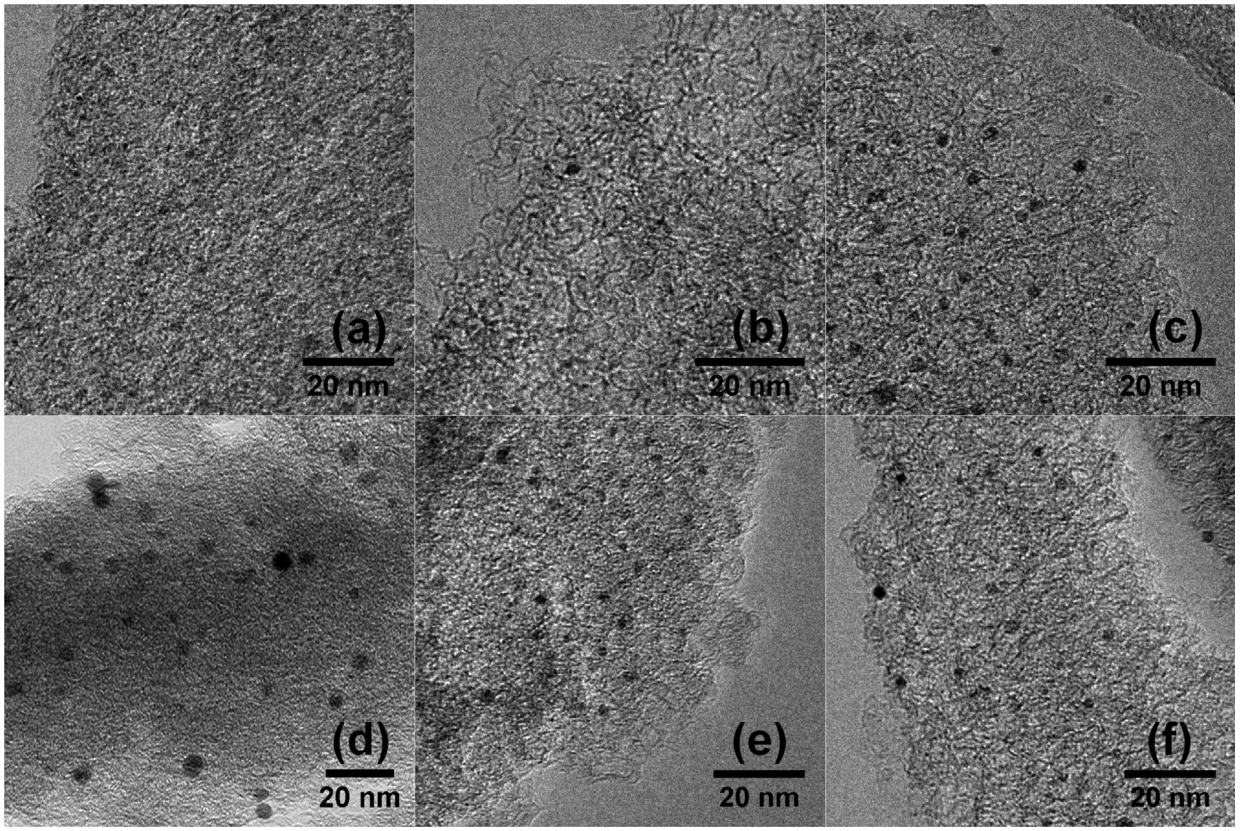

Fig. 1. Representative TEM images of (a) Pt/C(400), (b) Pt/C(600) (c) Pt/C(800), (d) Pt/C(1000), (e) Pt/C(800)–Re(300) and (f) Pt/C(800)–Re(600).

columns. The carbon product selectivities were calculated by:

$$S_i(\%) = \frac{\text{mol of product}_i \text{ formed} \times \text{number of C atoms}}{\text{mol of glycerol in the feed} \times \text{conversion} \times 3} \times 100$$

2.3.2. Water–gas shift reaction (WGS)

WGS reaction experiments were performed in a microreactor system [25]. Steam was supplied by evaporation of deionized water in a CEM unit in combination with a liquid flow controller. Gas flows were controlled by thermal mass flow controllers. All tubings were kept above 100 °C after the point of steam introduction. The dry product gas mixture was analyzed by an online gas chromatograph (Interscience CompactGC) equipped with Porapak Q and Molecular sieve 5A columns using thermal conductivity detectors. Experiments were carried out in a mixture of 2.5 vol% CO and 7.5 vol% H_2O balanced by He in the temperature range 150–400 °C. Typically, the catalyst was diluted with an appropriate amount of SiC of the same sieve fraction. The material was contained between two quartz wool plugs in a quartz reactor. Prior to catalytic activity measurements, the catalyst was reduced in a 20 vol% H_2/He flow (5 °C/min) to 300 °C for 30 min. The reactor was cooled in He to the reaction temperature. The catalyst was exposed to the reaction mixture for 10 min prior to the start of recording product gas mixture. At each reaction temperature, the CO conversion was followed for 1.5 h.

2.3.3. Acetaldehyde decomposition

Acetaldehyde decomposition experiments were performed in a continuous flow reactor setup. Hydrogen and acetaldehyde were fed as the feed components. Acetaldehyde was fed by bubbling He through a saturator kept at such a temperature to obtain a gas-phase acetaldehyde concentration of 3 vol%. Samples were first reduced at 300 °C. The reaction was carried out at 225 °C for 15 h. The reactor effluent was analyzed by online gas chromatography (Interscience GC-8000 Top, permanent gases on Shincarbon ST80/100 packed column connected to a TCD and hydrocarbons on a RT—Q bond column connected to a FID).

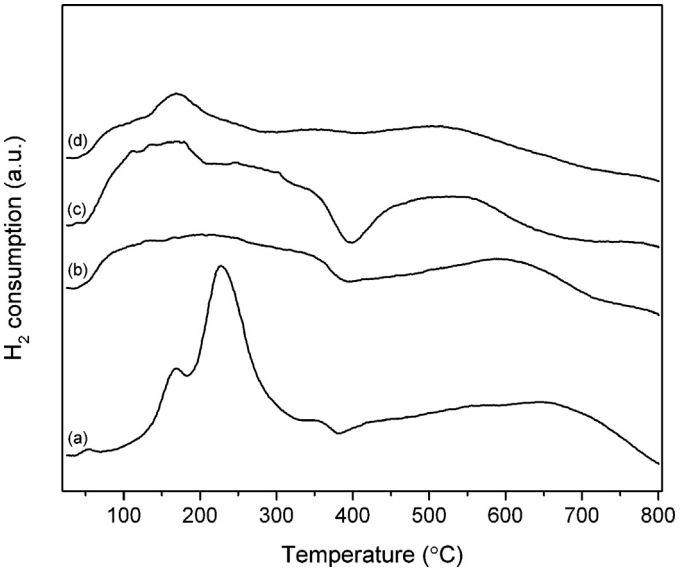

Fig. 2. TPR profiles of (a) Pt/C, (b) Pt/C(400)–Re, (c) Pt/C(600)–Re and (d) Pt/C(800)–Re.

Table 1
Metal loadings and average particle sizes for the Pt/C–(Re) catalysts.

Catalyst	Metal loading (wt%)[a]		Pt/Re ratio	Average particle size[b]
	Pt	Re		(nm)
Pt/C(400)	2.27	–	–	1.2 ± 0.8
Pt/C(600)				1.6 ± 0.8
Pt/C(800)				2.0 ± 1.2
Pt/C(1000)				4.2 ± 1.4
Pt/C(400)–Re(300)	2.19	3.51	0.60	1.3 ± 1.1
Pt/C(400)–Re(600)				1.3 ± 1.1
Pt/C(600)–Re(300)	2.19	3.85	0.54	1.5 ± 1.1
Pt/C(600)–Re(600)				1.3 ± 0.7
Pt/C(800)–Re(300)	2.19	3.54	0.59	2.6 ± 1.1
Pt/C(800)–Re(600)				2.5 ± 1.2

[a] Determined by ICP analysis.
[b] Determined by TEM analysis of the reduced and passivated catalysts.

3. Results and discussion

This section is organized in the following manner. In Section 3.1, we describe the characterization results of reduced Pt and Pt–Re catalysts. In Section 3.2, we discuss their catalytic performance in the APR reaction of glycerol, the WGS reaction and acetaldehyde decomposition. The latter two reactions serve as model reactions for some of the important elementary reaction steps in glycerol APR. For each reaction, we first discuss the influence of Pt particle size for Pt/C and then the catalytic data for the bimetallic Pt/C–Re catalysts.

3.1. Catalyst characterization

The metal loadings of the mono- and bimetallic catalysts as determined by ICP analysis are shown in Table 1. The Pt content of the parent Pt/C catalyst, which was prepared by incipient wetness impregnation, was 2.3 wt%. The Pt-to-Re molar ratio of the bimetallic catalysts was found to be close to the targeted value of 0.6. TEM analysis of the Pt/C catalysts shows that the Pt particles in the monometallic catalysts became larger with increasing reduction temperature (Fig. 1 & Table 1). Pt/C(400) contained the smallest Pt particles with an average size of 1.2 nm. Reduction at 600 and 800 °C led to modest increases of the average particle size to 1.6 and 2.0 nm, respectively; the average particle size increased more substantially to 4.2 nm after reduction at 1000 °C. TEM analysis of the bimetallic catalysts did not allow to draw conclusions on significant changes of the average particle size upon Re addition (Table 1). This is due to the distribution in the sizes of the supported Pt(Re) nanoparticles. The differences between 300 °C and 600 °C reduction of the freshly prepared Pt/C–Re catalysts was also very small.

H_2–TPR was used to follow the reduction of the Pt/C–(Re) catalysts (Fig. 2). The metal precursor in all catalysts was reduced below 300 °C, in agreement with literature [20,26]. The weak broad features starting above 400 °C and extending up to 800 °C observed for these catalysts are due to reduction of the oxygen functionalities of the activated carbon support [20]. The reduction features in the TPR patterns of the bimetallic Pt/C–Re catalysts prepared by the catalytic reduction method are substantially lower than those seen for PtRe/C prepared by sequential impregnation [20]. This difference is caused by the reduction of Pt/C prior to catalytic reduction deposition of $HReO_4$.

X-ray absorption near-edge spectra at the Pt L_{III} and Re L_{III} edges were recorded for catalysts that were reduced at 300 °C (Figs. 3 and 4). The spectra of the Pt/C catalysts closely resemble the spectrum of the Pt foil. This also holds for the bimetallic catalysts. For the bimetallic Pt/C–Re catalysts, the Re L_{III} near-edge spectra show small shifts in the edge energy (1.2–1.7 eV) compared with the spectrum of reference Re powder. These shifts are similar to what we reported for a PtRe/C catalyst in our previous study [20]. Such small shifts in the Re L_{III} edge XANES spectra are typically attributed to the presence of a small portion of Re in a slightly oxidized state, possibly because the Re atoms are not in contact with Pt [20,27,28]. The shift may also be due to the higher electronegativity of Pt compared with Re. The Fourier transforms of the EXAFS spectra at the Pt L_{III} edge show the presence of a single Pt–Pt shell for all four Pt catalysts (Table 2, Fig. S1). The coordination number of the Pt–Pt shell (CN_{Pt-Pt}) increased with reduction temperature, in line with the Pt particle size trend derived from TEM analysis. Consistent with the increasing CN, the Pt–Pt bond distance in the nanoparticles also increased. We estimated the average Pt particle size from CN_{Pt-Pt} using the approach developed by others [29–32]. For Pt/C reduced at 400, 600, 800 and 1000 °C, the EXAFS-derived average Pt particle sizes were 0.8, 1.0, 1.2 and 2.5 nm, respectively. Although trendwise the results are consistent with the TEM data, the EXAFS-derived particle sizes were lower than the TEM-derived values; such differences have been reported before in literature [29].

When Re is added to the reduced Pt/C catalysts, CN_{Pt-M} and CN_{Re-M} increased with increasing reduction temperature of the parent Pt/C catalyst. As discussed earlier [33], EXAFS cannot distinguish between Pt and Re backscatterers so that M in Pt–M and Re–M represents the sum of Pt and Re neighboring atoms. The values of CN_{Pt-M} for the bimetallic nanoparticles were similar to those determined for the monometallic catalysts. The CNs of the Re–M shells increased from 5.3 to 5.9 as with an increase in the reduction temperature of the parent Pt/C catalyst from 400 to 800 °C. This suggests that the Re shell formed around Pt slightly increased in size as the Pt nanoparticle core became larger.

3.2. Catalytic activity measurements

3.2.1. Aqueous phase reforming of glycerol

The Pt/C–(Re) catalysts were evaluated for their activity in the glycerol APR at 225 °C. Fig. 5 shows the conversion of glycerol as a function of the reaction time. The conversion of the Pt/C catalysts strongly depended on the average Pt particle size. Notably, the

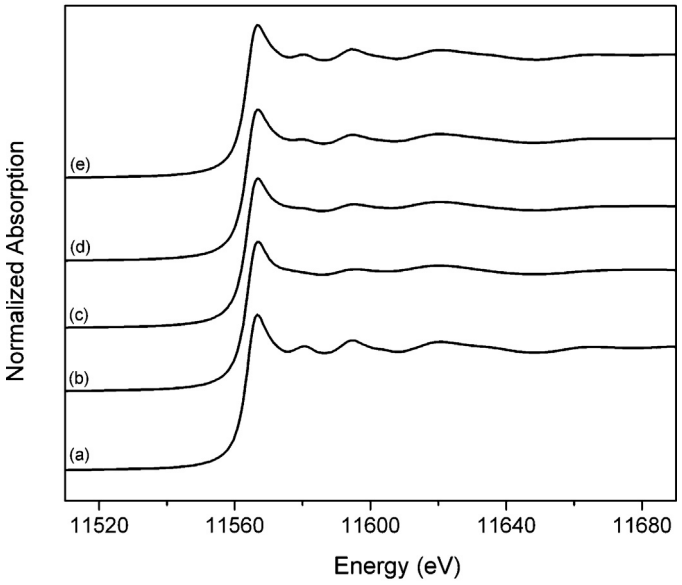

Fig. 3. Pt L_{III}-edge XANES spectra of (a) Pt foil, (b) Pt/C(400), (c) Pt/C(600), (d) Pt/C(800) and (e) Pt/C(1000). All catalysts were reduced at 300 °C before recording the XANES spectra.

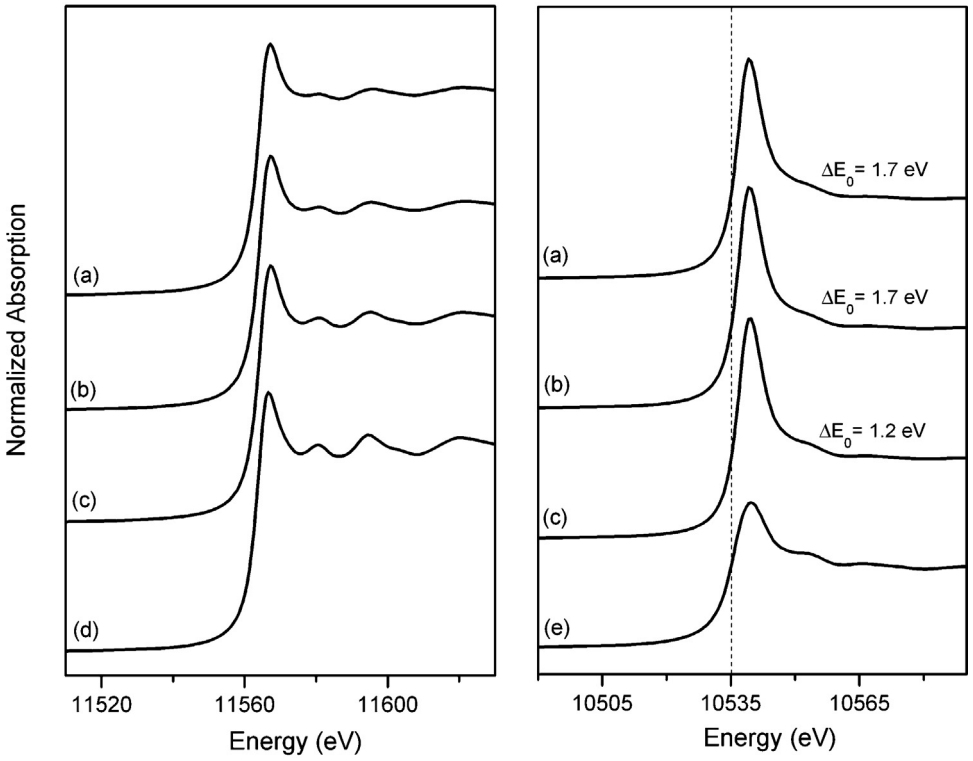

Fig. 4. Pt L_{III}-edge (left) and Re L_{III}-edge (right) XANES spectra of (a) Pt/C(400)–Re(300), (b) Pt/C(600)–Re(300), and (c) Pt/C(800)–Re(300) reduced at 300 °C. XANES spectra of (d) Pt foil and (e) Re powder (E_0 = 10535.2 eV) are plotted as references.

Table 2
Fit parameters of k^3-weighted EXAFS spectra at the Pt L_{III}-edge of Pt/C–(Re) catalysts reduced at 300 °C. M represents the backscatterer atom (Pt or Re).

Catalyst	EXAFS analysis				
	Shell	R (Å)	CN	$\Delta\sigma^2$ (Å^2)	E_0 (eV)
Pt/C(400)	Pt–Pt	2.685	6.3	0.010	−3.3
Pt/C(600)	Pt–Pt	2.719	7.2	0.011	−7.1
Pt/C(800)	Pt–Pt	2.755	7.7	0.008	−10.0
Pt/C(1000)	Pt–Pt	2.763	10	0.008	−10.5
Pt/C(400)–Re(300)	Pt–M_{Pt}[a]Re–M_{Re}[a]	2.7152.656	5.85.3	0.0090.007	−8.8−3.2
Pt/C(600)–Re(300)	Pt–M_{Pt}[a]Re–M_{Re}[a]	2.7272.662	6.85.5	0.0090.007	−9.5−4.1
Pt/C(800)–Re(300)	Pt–M_{Pt}[a]Re–M_{Re}[a]	2.7472.682	8.15.9	0.0080.007	−10.5−6.8

[a] A single shell was used for the first metal coordination shell, which represents the sum of Pt and Re atoms (note that Pt and Re backscatters cannot be distinguished). The subscript indicates the actual backscattering metal used in the EXAFS fit procedure.

Table 3
Glycerol conversion, rates, product selectivities, yield of H_2 and CO_2 in the glycerol APR reaction for the Pt/C–(Re) and Pt(Re)/C catalysts (T = 225 °C).

Catalyst	Time	$X_{glycerol}$	TOF_{H_2}[a]	Selectivity (%)								Y_{H_2}	Y_{CO_2}	C—O/C—C
	(min)	(%)	(mol/mol–$Pt_{surface}$ h)	CO_2	CH_4	C_2H_6	C_3H_8	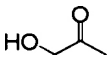	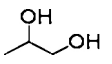	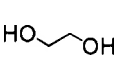	Others[b]	(%)	(%)	
Pt/C(400)	380	6.0	121	38.8	6.2	7.8	2.2	24.9	16.9	1.0	2.2	9.6	7.7	0.8
Pt/C(600)	200	6.4	479	41.5	6.0	4.1	0.9	18.4	25.1	2.1	1.9	14.9	8.7	0.6
Pt/C(800)	140	7.8	1072	44.3	2.8	1.9	0.8	14.7	30	3.0	2.5	18.7	11.2	0.5
Pt/C(1000)	200	8.7	826	21.0	0.7	1.0	1.2	42.4	27.6	2.6	3.5	9.8	6.5	1.3
Pt/C(400)–Re(300)	200	6.5	199	36.4	4.9	10.5	5.7	19.7	17.4	1.8	3.6	7.9	7.7	0.9
Pt/C(400)–Re(600)	320	6.8	123	33.5	5.7	11.4	4.6	23.0	16.8	1.4	3.6	7.8	7.5	1.1
Pt/C(600)–Re(300)	260	6.3	148	31.1	4.7	11.5	5.7	23.3	18.5	1.8	3.4	6.6	6.4	1.2
Pt/C(600)–Re(600)	200	6.1	174	27.9	4.2	8.7	4.8	32.2	16.3	1.6	4.3	6.9	5.5	1.2
Pt/C(800)–Re(300)	320	6.2	158	18.5	1.6	6.7	4.5	55.0	10.1	1.1	2.5	5.0	3.1	1.9
Pt/C(800)–Re(600)	320	4.7	70	15.2	1.4	6.1	4.4	54.2	13.8	1.4	3.5	2.3	2.3	2.3
PtRe(1:2)/C[c]	80	8.0	414	23.5	2.3	6.8	4.6	15.1	33.6	4.2	9.9	6.6	6.0	1.4

[a] Turnover frequency (±5%): H_2 formation rate per mol–$Pt_{surface}$ (average particle size from TEM analysis; activity of Re is minimal [20]) during APR reaction.
[b] Other products include alcohols (methanol, ethanol, 1-propanol, 2-propanol), acids (acetic acid, propanoic acid) and CO, propionaldehyde, 1,3-propanediol.
[c] Data taken from Ref. [20].

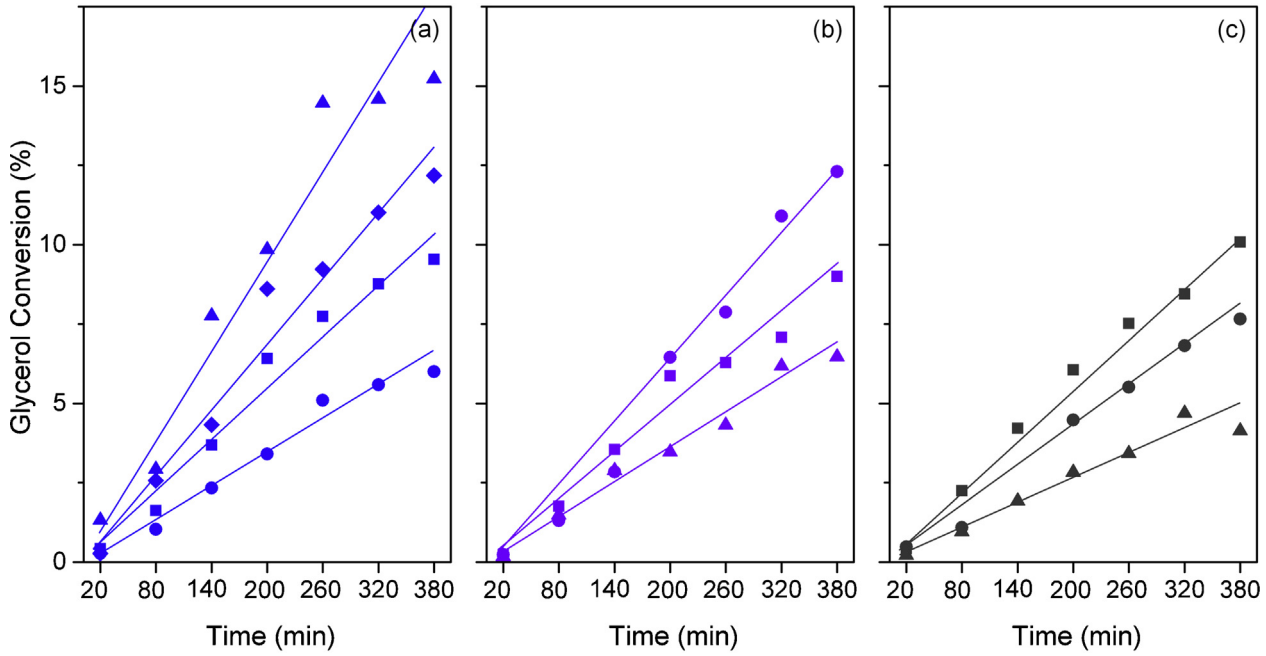

Fig. 5. Glycerol conversion in APR at 225 °C over (a) Pt/C(400) (◯), Pt/C(600) (▭), Pt/C(800) (△), Pt/C(1000) (◊), (b) Pt/C–Re(300) and (c) Pt/C–Re(600). Color symbols: Pt/C: blue, Pt/C–Re(300): purple and Pt/C–Re(600): gray. All catalysts were reduced at 300 °C prior to reaction. (For interpretation of the references to color in this figure legend, the reader is referred to the web version of this article.)

glycerol conversion was the highest for Pt/C(800) containing ~2 nm particles, which is about three times higher than that for Pt/C(400). The APR reaction mechanism is usually considered to proceed *via* two main routes (Scheme 1). The dehydration pathway starts with the dehydration (C—O cleavage) of glycerol. Hydrogenation of the unsaturated intermediate leads to diols, and *via* similar further reactions to monofunctional alcohols and alkanes. The decarbonylation pathway mainly generates CO and ethylene glycol. Due to the low temperature and high water activity, nearly all CO is converted to CO_2 and H_2 by the WGS reaction [2]. The APR conversion, activity and selectivity for all catalysts are given in Table 3 (detailed product distributions as a function of time on stream are given in the Supporting information). The data in Table 3 report selectivities at a glycerol conversions close to 6%, faciliting a reasonable discussion of the relevance of different reaction pathways in APR. Carbon-supported Pt nanoparticles with a size of 2 nm exhibited optimum activity towards H_2. The selectivity towards hydroxyacetone shows a minimum with particle size, opposite to the selectivity trend in 1,2-PDO and ethylene glycol. The latter finding implies that the decarbonylation rate increased with Pt particle size up to a maximum of ~2 nm in Pt/C(800). In line with this trend, the ratio of formation of C—O/C—C cleavage products was highest for Pt/C(400) and Pt/C(1000) with the smallest and largest Pt particles, respectively. Lehnert and Claus reported increasing H_2 turnover frequencies with increasing Pt particle size in glycerol APR [6]. Kirilin et al. found similar increasing trends in xylitol APR over a set of Pt nanoparticles supported on various carbon materials [34].

The addition of Re to the Pt/C catalysts reduced at different temperatures had significant influence on the catalytic performance. After 320 min on stream (Fig. 5), the glycerol conversion for Pt/C(400)–Re(300) was nearly two times higher than that for the parent Pt/C(400) catalyst. The increase in glycerol conversion after 320 min on stream for Pt/C(400)–Re(600) was much smaller than for Pt/C(400)–Re(300). For the Pt/C catalysts initially reduced above 400 °C, Re addition decreased the catalytic activity. This decrease became more significant for Pt/C catalysts containing larger Pt particles. The temperature of the Re reduction step had only a small influence on the catalytic activity. Regarding the product

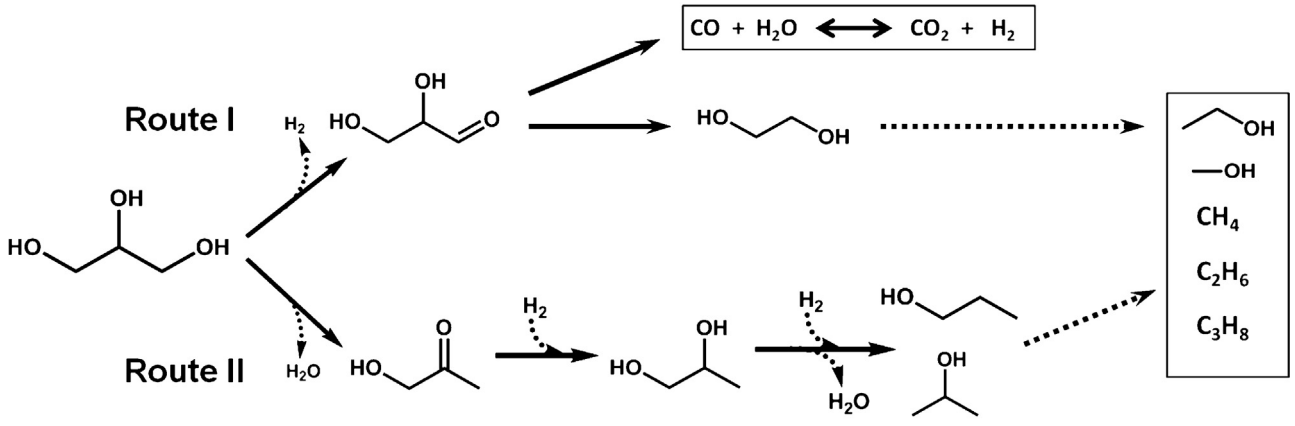

Scheme 1. Reaction pathways of glycerol reforming on PtRe catalysts in the aqueous phase.

Table 4
WGS reaction rates for Pt/C–(Re) and Pt(Re)/C catalysts (T = 225 °C, GHSV = 1×10^5 ml/g_{cat} h, H_2O/CO = 3).

Catalyst	r(WGS)[a] (mol/mol–(Pt + Re) h)	$r(WGS)_{PtRe}/r(WGS)_{Pt}$[b]	TOF_{WGS}[a] (mol/mol–$(Pt + Re)_{surface}$ h)
Pt/C(400)	1	–	1
Pt/C(600)	11.5	–	16
Pt/C(800)	25.5	–	45
Pt/C(1000)	10.3	–	38
Pt/C(400)–Re(300)	14.6	14.6	–
Pt/C(400)–Re(600)	39.1	39.1	–
Pt/C(600)–Re(300)	53.5	4.7	–
Pt/C(600)–Re(600)	73	6.3	–
Pt/C(800)–Re(300)	67.8	2.7	–
Pt/C(800)–Re(600)	89.7	3.5	–
PtRe(1:2)/C[c]	14.6	10.4	–

[a] Rate and turnover frequency (±5%): CO consumption rate per mol–Pt + Re and mol–$Pt + Re_{surface}$, respectively, (average particle size from TEM analysis; activity of Re must be taken into account [20], hence Pt + Re) during WGS reaction.
[b] Pt reference data on the basis of the same reduction temperature of the Pt/C precursor.
[c] Data taken from Ref. [20].

selectivities, the ratio of products formed *via* C—O bond cleavage to those formed *via* C—C bond cleavage reactions was higher for the Pt/C–Re catalysts than for the parent Pt/C catalysts (Table 3). This trend points to higher rates of dehydration reactions for the bimetallic catalysts. The increase of the rate of C—O bond cleavage upon alloying Pt with Re is consistent with the proposal that Brønsted acid sites are generated in bimetallic PtRe catalysts under APR conditions [19,20]. This explains the increase in higher alkanes (ethane and propane) selectivities upon Re alloying. Note the effect of Re on the formation of alkanes decreased as Re was added to larger Pt particles (Table 3). The Pt/C(800)–Re catalysts, which were the least APR active among the Pt/C–Re catalysts, showed lower selectivities towards alkanes when compared with the other bimetallic catalysts with smaller Pt particles. These catalysts showed about 50% selectivity towards hydroxyacetone. This stems from the very low rate of hydrogenation of hydroxyacetone to 1,2-PDO as well as its further dehydration to alkanes. Chia et al. recently reported similar observations for RhRe/C catalysts used for aqueous phase hydrogenolysis of 2-(hydroxymethyl)tetrahydropyran [35]. They mentioned the formation of RhRe nanoparticles with Rh-rich cores and a shell of metallic Re islands. An important finding in the work of Chia et al. was that the increase in the coordination number of Re with increasing reduction temperature led to a decrease in the concentration of acid sites and a consistent decrease in C—O hydrogenolysis activity of the RhRe/C catalysts [35]. Similarly, in the current study, deposition of Re on larger Pt particles resulted in an increase in $CN_{Re–M}$. This may relate to the decrease in the number of active sites for hydrogenolysis reactions. In general, an increase in the reduction temperature of Pt/C–Re catalysts from 300 to 600 °C resulted in a decrease in the APR activity.

3.2.2. Water–gas shift reaction

Fast removal of CO from the catalyst surface by the WGS reaction was argued to be important to maintain high APR activities [12,18,26]. Arrhenius plots for the WGS reaction of Pt/C–(Re) catalysts are given in Fig. S2. Representative activity data are listed in Table 4. The particle size had a strong influence on the WGS activity for the Pt/C catalysts. The WGS rate was highest at the intermediate Pt nanoparticle size of 2 nm. Although these results were obtained in the gas phase, the trend correlates well with the TOF_{H_2} trend of glycerol APR for the monometallic catalysts. Addition of Re to the reduced Pt/C catalysts resulted in significantly higher WGS rates. For the Pt/C–Re catalysts reduced at 300 °C, the promotional effect was highest for Pt/C(400) and decreased with increasing particle size of the parent Pt/C catalyst. An increase in the reduction temperature of Pt/C–Re catalysts from 300 °C to 600 °C further enhanced the activity. This suggests that higher reduction temperature of the freshly prepared Pt/C–Re catalyst resulted in increased Pt–Re synergy in the WGS reaction.

It is well known that the strong adsorption of CO on Pt surfaces leads to severe reaction inhibition at low reaction temperatures. A high rate of adsorbed CO removal as CO_2 by reaction with O and OH surface intermediates will increase the overall catalytic activity during APR. The microkinetic model of Mavrikakis' group based on DFT-computed kinetic parameters for the Pt(111) surface shows that the WGS reaction preferentially proceeds through a COOH surface intermediate formed by reaction between adsorbed CO and OH. Water activation, *i.e.*, $H_2O_{ads} \rightarrow OH_{ads} + H_{ads}$, was proposed as the rate-controlling step for Pt(111) [36]. Brønsted–Evans–Polanyi (BEP) relations [37] predict that the activation barrier of water activation will depend on the metal —OH bond strength [38]. An increase of the metal —OH bond strength lowers the reaction barrier. The metal —OH bond strength of 346 kJ/mol for Re(0001) is higher than the corresponding value of 282 kJ/mol for Pt(111). As a result, the formation of OH_{ads} is slightly endothermic for Pt(111) and exothermic for Re(0001) [20,39]. Accordingly, BEP relations predict that the initial water activation step is kinetically favored for the close-packed Re surface. In line with this, we found that Re/C is a more active WGS catalyst than Pt/C [20]. From the data in the present study, a more complex picture emerges in that Re/C is more active than Pt/C when the latter catalyst is reduced at 400 °C, whereas Pt/C reduced at a temperature of 600 °C or higher is more active than Re/C. This is due to the strong size dependence of carbon-supported Pt nanoparticles in the WGS reaction. We interpret this particle size effect in terms of step-edge sites facilitating water activation. Quantum-chemical calculations of Zhu et al. showed that O and OH binds stronger on a stepped Pt(210) surface than on Pt(111) [39], so that in line with BEP considerations the overall barrier for OH_{ads} formation should be more favorable for corrugated surfaces than for the close-packed Pt(111) surface. This is consistent with values for the activation barrier for water activation of 53 and 87 kJ/mol for Pt(210) and Pt(111), respectively. This particle size dependence also agrees with the literature discussing the decrease of the number of step-edge sites when the particle size becomes smaller than *ca.* 2 nm [40].

It is seen from Table 4 that addition of Re to the Pt/C catalysts resulted in higher WGS rates. The rate differences between the Pt/C–Re catalysts tend to be smaller than those between the parent Pt/C catalysts. As Re is a more reactive metal than Pt, Re will facilitate the water activation step in Pt–Re alloys [37]. Despite the formation of a Re shell around the Pt nanoparticles, it is likely that the subsequent reduction step resulted in some rearrangement

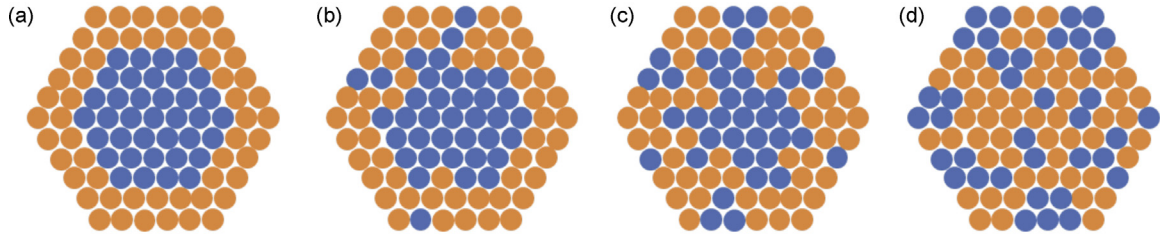

Scheme 2. Schematic representation of the bimetallic nanoparticles prepared by catalytic reduction of ReO_4 on reduced Pt/C: (a) as-prepared Pt/C–Re, (b) Pt/C–Re reduced at 300 °C, (c) Pt/C-Re reduced at 600 °C and (d) PtRe/C prepared by conventional incipient wetness impregnation and reduction. Color atoms: Pt: blue; Re: orange. (For interpretation of the references to color in this figure legend, the reader is referred to the web version of this article.)

of the two metals in the particles. Indeed, a pure Re coating on a Pt nanoparticle would not be expected to give rise to the activity increase, as Re itself exhibited much lower WGS activity than the alloys. As we have found that alloying with Re strongly increased the WGS activity of Pt/C, a reasonable explanation is that the final reduction step of the bimetallic catalyst led to the appearance of Pt atoms at the nanoparticle surface. In a microkinetic model of the WGS reaction for bimetallic PtRe, Zhu explained increased WGS activity by Re surface atoms being mainly covered by O_{ads} and OH_{ads} and Pt surface atoms providing centers for CO adsorption [41]. Thus, the higher WGS rate of Pt–Re alloys reduced at 600 °C compared with 300 °C is likely due to the higher fraction of Pt atoms at the surface (Scheme 2). Consistent with this, Pt/C(400)–Re(600) is more active than a PtRe/C catalyst prepared in a conventional manner (Table 4). The smaller variation in the catalytic WGS performance of the Pt/C–Re set as compared with the Pt/C set can be explained as follows. For Pt/C, water activation is strongly size dependent because of the low rate of water activation. In Pt–Re alloys, on the other hand, Re facilitates water activation and the overall reaction will depend less significantly on the particle size. We excluded by *in-situ* XAS that the WGS reaction led to significant changes in the oxidation state and coordination numbers of Pt and Re (Figs. S3–6, Table S11). We observed that the Pt/C catalysts were stable, whereas the Pt/C–Re catalysts, irrespective of particle size, became ~30% less active when the temperature was decreased from 400 °C to 130 °C (not shown). This suggests that small changes in the surface composition may occur. In earlier work [11], Pt(Re) catalysts on oxide supports became more active during the decreasing temperature branch, which was possibly the result of further reduction under WGS conditions. It signifies that our catalysts are well reduced.

3.2.3. Acetaldehyde decomposition

The rate of acetaldehyde decomposition of the Pt and their Re-alloyed counterparts was investigated in order to determine their activity in a model reaction in which only C—C bond cleavage is involved (no C—O bond cleavage). The reaction was carried out in the gas phase and hydrogen was added to the reaction mixture to avoid undesired deactivation by extensive carbon lay-down. No catalyst deactivation was observed during the course of the catalytic activity measurements. The main reaction products were CO and CH_4; ethanol was observed in small quantities. Ethanol is the product of acetaldehyde hydrogenation. The activity results collected in Table 5 show that the CO yield for Pt/C catalysts did not significantly vary when the catalysts were reduced at 800 °C or below. The nearly constant CO yield for these Pt/C catalysts points to an increase of the intrinsic rate of acetaldehyde decomposition with increasing Pt particle size in the 1.2–2 nm range. The larger particles in Pt/C(1000) had a lower activity. The particle size dependence of acetaldehyde trended well with the dependence of the WGS reaction. Candidate intermediates to undergo C—C bond cleavage are CH_x—CO species; CH—CO is the most likely one, as proposed by Wang and Liu for Pt(100) [42]. The dissociation of CH_x—CO proceeds through late transition states and, hence, we may predict that the barrier for C—C bond cleavage will decrease with increasing bond energy of the CH_x and CO fragments. This implies that open and corrugated surfaces will favor C—C bond cleavage. Consistent with this, Zhu et al. found that the barrier for cleavage of the C—C bond in CH—CO is 57 kJ/mol on the (520) facet of Pt [41], whereas the barrier is much higher for the (111) facet with values of 93 kJ/mol reported by Wang et al. [42] and Sutton et al. [43]. Accordingly, we infer that the similar particle size dependence for WGS and C—C bond cleavage reactions relates to the preference for these reactions to occur on step-edge sites of the Pt surface.

Upon addition of Re to Pt/C reduced at 400, 600 and 800 °C, the acetaldehyde conversion was seen to increase. The promoter effect was smaller than observed for the WGS reaction. For instance, by comparing the CO yields it is noted that the Pt/C(400)–Re and Pt/C(600)–Re catalysts exhibited ~1.5 times higher activities than the corresponding parent Pt/C catalysts. The activity of

Table 5
Acetaldehyde conversion, rates, yield and selectivity of CO in the C_2H_4O decarbonylation reaction for Pt/C–(Re) and Pt(Re)/C catalysts (T = 225 °C, GHSV = 7200 $ml_{acetaldehyde}/g_{cat}$ h; gas-phase composition H_2:C_2H_4O = 1:1 by volume with balance He).

Catalyst	$X_{C_2H_4O}$[a] (%)	r (C_2H_4O)[b] (mol/mmol–Pt h)	$TOF_{C_2H_4O}$[b] (mol/mol–$Pt_{surface}$ h)	Y_{CO}[a] (%)	S_{CO}[a] (%)
Pt/C(400)	19.6	0.6	209	9.7	50
Pt/C(600)	20.3	0.6	290	10.1	50
Pt/C(800)	19.9	0.6	351	9.8	49
Pt/C(1000)	9.7	0.3	331	4.4	46
Pt/C(400)–Re(300)	37.9	1.2	339	15.1	40
Pt/C(600)–Re(300)	39.1	1.2	373	14.4	37
Pt/C(800)–Re(300)	28.4	0.9	431	9.6	34
PtRe(1:2)/C[c]	41.2	1.1	381	17.2	42

[a] Average of at least 4 h time on stream.
[b] Rate and turnover frequency (±5%): CO formation rate per mmol–Pt and mol–$Pt_{surface}$, respectively, (average particle size from TEM analysis; Re is inactive [20]) during acetaldehyde decomposition.
[c] Data taken from Ref. [20].

Pt/C(800)–Re(300) was similar to the activity of Pt/C(800). We earlier found that Re/C was not active in this reaction, which most likely stems from carbon poisoning [20]. The much higher activity of the herein prepared Pt/C–Re catalysts by the catalytic reduction method suggests that the nanoparticles have a surface composition different from a pure Re skin around the Pt nanoparticles. The presence of Pt at the surface is further underpinned by the much higher hydrogenation activity of acetaldehyde to ethanol as compared with the parent Pt/C catalysts; this is consistent with the notion that supported PtRe are better hydrogenation catalysts than Pt [20]. The shift in acetaldehyde conversion towards hydrogenation for larger Pt–Re nanoparticles can also be traced in the glycerol APR data with Pt/C(800)–Re(300) exhibiting relatively low glycerol conversion rate and H_2 yield.

3.2.4. Overall discussion

Values for the TOF normalized per surface atom (Pt and Pt + Re, the latter assuming that Re is also active in the reaction) for Pt/C catalysts are provided in Tables 3–5. The TOF for H_2 production rate in APR is highest for on average 2 nm Pt particles consistent with the TOF trends observed in separate model WGS and acetaldehyde decomposition measurements. The removal of CO by the WGS reaction resulted in increased overall glycerol conversion rates (not shown). The increased C—C bond cleavage activity favored complete reforming over dehydration-hydrogenation reactions to alcohol intermediates and alkane end-products. These trends are attributed to the higher density of step-edge sites on the surface of larger Pt particles.

The addition of Re considerably affected the APR performance. It strongly improved the activity of Pt/C(400), whilst the Pt/C(600) was unchanged and Pt/C(800) became less active (Fig. 5; Table S1). Table 3 also contains data of a PtRe(1:2)/C catalyst prepared by conventional methods, that is impregnation and drying of the Pt precursor followed by Re precursor ($HReO_4$) loading [20]. Reduction of this catalyst was done at 300 °C. The synergy between Pt and Re for the conventional catalyst was greater than for the set of catalysts prepared by the catalytic reduction method (see Table S1). The difference can be related to the preparation procedure. The catalytic reduction method initially deposits a shell of Re around the reduced Pt nanoparticles, whereas reduction of the sequentially impregnated PtRe/C catalyst will result in a less ordered distribution of Pt and Re in the final nanoparticles (Scheme 2). The elementary reaction steps giving rise to C—O and C—C bond cleavage are expected to require Pt ensembles, because Re ensembles may be presumed to be covered by oxygen or hydroxyl groups under APR reaction conditions. We stress the difference in reaction conditions for the WGS and acetaldehyde model reactions and the APR reaction. The trends in the WGS and acetaldehyde decomposition model reaction data suggest that (i) a small fraction of Pt was present as isolated atoms at the surface of the metal nanoparticles and (ii) the hydrogenation activity of the alloy was higher than that of Pt and Re [20]. Thus, we argue that the much lower activity in APR after 320 min (Table S1) of Pt/C(400)–Re(300) compared with a reference PtRe/C catalyst is due to lower Pt surface atom content. The less pronounced and even negative effect of Re addition for larger Pt nanoparticles, *i.e.,* Pt/C(600) and Pt/C(800), should be due to the formation of a thicker Re shell around larger nanoparticles; this results in a smaller amount of Pt atoms at the nanoparticle surface upon reduction, and a decreased likelihood of Pt ensembles large enough to catalyze the bond breaking reactions involved in APR. For the bimetallic catalyst with the largest particles tested in APR *i.e.,* Pt/C(800)–Re(600), the C—O/C—C bond cleavage ratio was the highest, consistent with the predominance of Re at the catalytic surface. Another interesting observation is that the hydrogenation of hydroxyacetone to 1,2-PDO during glycerol APR decreased with increasing Pt(-Re) particle size (Table 3), whereas the hydrogenation of acetaldehyde to ethanol trended oppositely (*cf.* the decreased CO selectivity in Table 5). Re sites will be covered by OH surface intermediates under APR conditions, while such intermediates are absent in the acetaldehyde model reaction experiments. Thus, the hydrogenation activity of Pt–Re increased with increasing Re enrichment of the surface, but this effect was not seen in the APR data because of increasing OH surface coverage with particle size.

Summarizing, the APR reaction of glycerol is strongly structure sensitive for Pt nanoparticle catalysts due to the importance of step-edge sites for water activation and C—C bond cleavage steps. For bimetallic Pt–Re catalysts, it can be inferred that the WGS reaction is preferred over Re-enriched surfaces, whereas the APR reaction requires Pt ensembles large enough to accommodate C—C and C—O bond cleavage reactions.

4. Conclusions

The APR activities of a set of carbon-supported Pt catalysts were found to be strongly dependent on the Pt particle size. Reduction at 400, 600, 800 and 1000 °C of a freshly prepared Pt/C catalyst resulted in average Pt particle sizes of 1.2, 1.6, 2.0 and 4.2 nm. Optimum TOF_{H_2}, yields of reforming products (H_2 and CO_2) as well as the C—C bond cleavage rates of the catalysts were found for Pt nanoparticles of intermediate particle size of ~2 nm. These trends agreed with differences in model gas-phase water–gas shift and acetaldehyde decomposition reactions. This is attributed to similar site requirements for these two reactions. Binding of O and OH species is stronger and the cleavage of C—C bonds of CH—CO intermediate occurs at higher rates on stepped Pt surfaces. Addition of Re on the reduced Pt/C catalysts following the catalytic reduction method resulted in an increase in the C—O bond cleavage products relative to the products from C—C bond cleavage reactions. The glycerol conversion in APR increased only for the Pt/C(400)–Re catalyst containing initially the smallest particles. For the other bimetallic Pt/C–Re systems, APR activity was typically lower than the parent Pt/C. It is due to the lower abundance of Pt on the surface of increasingly large Pt–Re particles. In acetaldehyde decomposition, the Re addition on large Pt particles resulted in increased C—C bond cleavage rates as well as increased hydrogenation rates to ethanol. The WGS activity of the Pt/C–Re catalysts increased substantially when compared to the Pt/C catalysts. The promotional effect of Re increased with increased Pt particle size and increasing reduction temperature of the Pt–Re alloys in WGS. These effects are related to the rearrangement of the particles and appearance of Pt atoms on the surface. For bimetallic catalysts the WGS reaction is preferred over Re-enriched surfaces, whereas the APR reaction requires Pt ensembles large enough to accommodate C—C and C—O bond cleavage reactions.

Acknowledgements

AC acknowledges support from the Eindhoven University of Technology in the framework of the European Graduate School on Sustainable Energy. The authors acknowledge a financial support from the European Institute of Innovation and Technology, under the KIC InnoEnergy Syncon project. We thank Mrs. Adelheid Elemans for the help with elemental analysis and Mr. Anton Litke and Mr. Arno van Hoof for the TEM recordings. We thank NWO-Dubble for access to X-ray absorption spectroscopy facilities at ESRF and ESRF staff for their support.

Appendix A. Supplementary data

Supplementary data associated with this article can be found, in the online version, at http://dx.doi.org/10.1016/j.apcatb.2015.02.027.

References

[1] R.R. Davda, J.W. Shabaker, G.W. Huber, R.D. Cortright, J.A. Dumesic, Appl. Catal. B 56 (2005) 171–186.
[2] A. Wawrzetz, B. Peng, A. Hrabar, A. Jentys, A.A. Lemonidou, J.A. Lercher, J. Catal. 269 (2010) 411–420.
[3] R.R. Davda, J.W. Shabaker, G.W. Huber, R.D. Cortright, J.A. Dumesic, Appl. Catal. B 43 (2003) 13–26.
[4] J.W. Shabaker, G.W. Huber, R.R. Davda, R.D. Cortright, J.A. Dumesic, Catal. Lett. 88 (2003) 1–8.
[5] G.W. Huber, J.W. Shabaker, S.T. Evans, J.A. Dumesic, Appl. Catal. B 62 (2006) 226–235.
[6] K. Lehnert, P. Claus, Catal. Commun. 9 (2008) 2543–2546.
[7] S.N. Delgado, D. Yap, L. Vivier, C. Especel, J. Mol. Catal. A 367 (2013) 89–98.
[8] A. Ciftci, B. Peng, A. Jentys, J.A. Lercher, E.J.M. Hensen, Appl. Catal. A 431 (2012) 113–119.
[9] A. Ciftci, D.A.J.M. Ligthart, E.J.M. Hensen, Green Chem. 16 (2014) 853–863.
[10] B. Meryemoglu, A. Hesenov, S. Irmak, O.M. Atanur, O. Erbatur, Int. J. Hydrogen Energy 35 (2010) 12580–12587.
[11] A. Ciftci, S. Eren, D.A.J.M. Ligthart, E.J.M. Hensen, ChemCatChem 6 (5) (2014) 1260–1269.
[12] Y. Guo, M.U. Azmat, X.H. Liu, Y.Q. Wang, G.Z. Lu, Appl. Energy 92 (2012) 218–223.
[13] G. Wen, Y. Xu, H. Ma, Z. Xu, Z. Tian, Int. J. Hydrogen Energy 33 (2008) 6657–6666.
[14] T. Miyazawa, S. Koso, K. Kunimori, K. Tomishige, Appl. Catal. A 318 (2007) 244–251.
[15] D.M. Alonso, S.G. Wettstein, J.A. Dumesic, Chem. Soc. Rev. 41 (2012) 8075–8098.
[16] D.L. King, L.A. Zhang, G. Xia, A.M. Karim, D.J. Heldebrant, X.Q. Wang, T. Peterson, Y. Wang, Appl. Catal. B 99 (2010) 206–213.
[17] S. Koso, H. Watanabe, K. Okumura, Y. Nakagawa, K. Tomishige, Appl. Catal. B 111 (2012) 27–37.
[18] E.L. Kunkes, D.A. Simonetti, J.A. Dumesic, W.D. Pyrz, L.E. Murillo, J.G.G. Chen, D.J. Buttrey, J. Catal. 260 (2008) 164–177.
[19] L. Zhang, A.M. Karim, M.H. Engelhard, Z.H. Wei, D.L. King, Y. Wang, J. Catal. 287 (2012) 37–43.
[20] A. Ciftci, D.A.J.M. Ligthart, A.O. Sen, A.J.F. van Hoof, H. Friedrich, E.J.M. Hensen, J. Catal. 311 (2013) 88–101.
[21] C.L. Pieck, P. Marecot, C.A. Querini, J.M. Parera, J. Barbier, Appl. Catal. A 133 (1995) 281–292.
[22] C.L. Pieck, P. Marecot, J. Barbier, Appl. Catal. A 134 (1996) 319–329.
[23] C.L. Pieck, P. Marecot, J. Barbier, Appl. Catal. A 143 (1996) 283–298.
[24] E.P. Maris, W.C. Ketchie, M. Murayama, R.J. Davis, J. Catal. 251 (2007) 281–294.
[25] D.A.J.M. Ligthart, R.A. van Santen, E.J.M. Hensen, Angew. Chem. Int. Ed. 50 (2011)
5306–5310.
[26] D.A. Simonetti, E.L. Kunkes, J.A. Dumesic, J. Catal. 247 (2007) 298–306.
[27] J. Sa, C. Kartusch, M. Makosch, C. Paun, J.A. van Bokhoven, E. Kleymenov, J. Szlachetko, M. Nachtegaal, H.G. Manyar, C. Hardacre, Chem. Commun. 47 (2011) 6590–6592.
[28] J.L. Xiao, R.J. Puddephatt, Coord. Chem. Rev. 143 (1995) 457–500.
[29] X.M. Wang, N. Li, Z.T. Zhang, C. Wang, L.D. Pfefferle, G.L. Haller, ACS Catal. 2 (2012) 1480–1486.
[30] S. Calvin, M.M. Miller, R. Goswami, S.F. Cheng, S.P. Mulvaney, L.J. Whitman, V.G. Harris, J. Appl. Phys. 94 (2003) 778–783.
[31] S. Calvin, S.X. Luo, C. Caragianis-Broadbridge, J.K. McGuinness, E. Anderson, A. Lehman, K.H. Wee, S.A. Morrison, L.K. Kurihara, Appl. Phys. Lett. 87 (2005) 233102–233103.
[32] S. Calvin, C.J. Riedel, E.E. Carpenter, S.A. Morrison, R.M. Stroud, V.G. Harris, Phys. Scr. T115 (2005) 744.
[33] O.M. Daniel, A. DeLaRiva, E.L. Kunkes, A.K. Datye, J.A. Dumesic, R.J. Davis, ChemCatChem 2 (9) (2010) 1107–1114.
[34] A.V. Kirilin, B. Hasse, A.V. Tokarev, L.M. Kustov, G.N. Baeva, G.O. Bragina, A.Y. Stakheev, A.R. Rautio, T. Salmi, B.J.M. Etzold, J.P. Mikkola, D.Y. Murzin, Catal. Sci. Technol. 4 (2014) 387–401.
[35] M. Chia, B.J.O. Neill, R. Alamillo, P.J. Dietrich, F.H. Ribeiro, J.T. Miller, J.A. Dumesic, J. Catal. 308 (2013) 226–236.
[36] L.C. Grabow, A.A. Gokhale, S.T. Evans, J.A. Dumesic, M. Mavrikakis, J. Phys. Chem. C 112 (2008) 4608–4617.
[37] M. van Santen, R.A. Neurock, Molecular Heterogeneous Catalysis: A Conceptual and Computational Approach, Wiley-VCH, Weinheim, 2007.
[38] P.W. van Grootel, E.J.M. Hensen, R.A. van Santen, Surf. Sci. 603 (2009) 3275–3281.
[39] T. Zhu, P.W. van Grootel, I.A.W. Filot, S.G. Sun, R.A. van Santen, E.J.M. Hensen, J. Catal. 297 (2013) 227–235.
[40] R.A. van Santen, Acc. Chem. Res. 42 (2009) 57–66.
[41] T. Zhu, PhD Thesis, Technische Universiteit Eindhoven, 2013, ISBN 978-90-386-3505-7.
[42] H.F. Wang, Z.P. Liu, J. Am. Chem. Soc. 130 (2008) 10996–11004.
[43] J.E. Sutton, P. Panagiotopoulou, X.E. Verykios, D.G. Vlachos, J. Phys. Chem. C 117 (2013) 4691–4706.